Chemical State Analysis of Phosphorus Performed by X-ray Emission Spectroscopy

ARTICLE *in* ANALYTICAL CHEMISTRY · APRIL 2015

Impact Factor: 5.64 · DOI: 10.1021/acs.analchem.5b00782 · Source: PubMed

6 AUTHORS, INCLUDING:

Marko Petric

Jožef Stefan Institute

4 PUBLICATIONS **0** CITATIONS

SEE PROFILE

Rok Bohinc

Paul Scherrer Institut

14 PUBLICATIONS **33** CITATIONS

SEE PROFILE

Klemen Bucar

Jožef Stefan Institute

64 PUBLICATIONS **543** CITATIONS

SEE PROFILE

Matjaž Kavčič

Jožef Stefan Institute

81 PUBLICATIONS **582** CITATIONS

SEE PROFILE

analytical chemistry

Article

pubs.acs.org/ac

Chemical State Analysis of Phosphorus Performed by X-ray Emission Spectroscopy

Marko Petric,*[,†,‡] Rok Bohinc,[†] Klemen Bučar,[†] Matjaž Žitnik,[†,§] Jakub Szlachetko,[∥,⊥] and Matjaž Kavčič*[,†]

[†]J. Stefan Institute, Jamova 39, SI-1000 Ljubljana, Slovenia

[‡]Jozef Stefan International Postgraduate School, Jamova cesta 39, 1000 Ljubljana, Slovenia

[§]Faculty of Mathematics and Physics, University of Ljubljana, Jadranska ulica 19, SI-1000 Ljubljana, Slovenia

[∥]Paul Scherrer Institute, CH-5232 Villigen PSI, Switzerland

[⊥]Institute of Physics, Jan Kochanowski University, Kielce, Poland

Supporting Information

ABSTRACT: An experimental and theoretical study of phosphorus electronic structure based on high energy resolution X-ray emission spectroscopy was performed. The Kα and Kβ emission spectra of several phosphorus compounds were recorded using monochromatic synchrotron radiation and megaelectronvolt (MeV) proton beam for target excitation. Measured spectra are compared to the results of ab initio quantum chemical calculations based on density functional theory (DFT). Clear correlation between energy position of the Kα emission line and the phosphorus formal oxidation state as well as DFT-calculated number of valence electrons is obtained; measured energy shifts are reproduced by the calculations. Chemical sensitivity is increased further by looking at the Kβ emission spectra probing directly the structure of occupied molecular orbitals. Energies and relative intensities of main components are given together with the calculated average atomic character of the corresponding molecular orbitals involved in transitions.

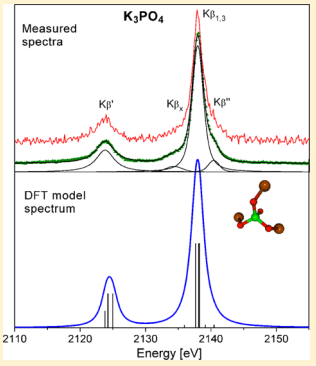

Phosphorus is an essential element for all living systems, being crucial in the transmission of chemical energy through the ATP molecule.[1] Marine primary production and distribution of plankton depend on the availability of phosphorus as a vital nutrient.[2] Buildup of phosphorus in excessively fertilized soil and its transfer to groundwater[3,4] and release of phosphorus in atmospheric aerosols[5] and marine environment[6] are only some of the important examples of environmental concerns related to the presence of different forms of phosphorus.

Due to its multivalent character, phosphorus forms chemical bonds with variety of atoms of different electronegativity, changing significantly the local electronic structure around the phosphorus atoms. Inner-shell X-ray spectroscopies, in particular X-ray absorption spectroscopy (XAS), are one of the most suitable techniques that can probe local electron density and configuration around the center atom. These days, this is a standard, well-matured spectroscopic technique implemented at the third-generation synchrotron radiation sources. X-ray absorption near-edge structure (XANES) spectroscopy has been used extensively to chemically specify phosphorus, especially in soils, biosamples, and minerals.[7−14]

High-resolution X-ray emission spectroscopy (XES) represents an alternative technique which can be used complementary to XANES spectroscopy to study electronic structure of materials. XES in the tender and hard X-ray range has been used to, for example, characterize geochemical systems,[15,16] probe metal−ligand interaction in coordination complexes,[17] study metalloproteins,[18] and also catalysts.[19] In contrast to XAS, XES is probing the occupied electronic levels below the Fermi level, yielding direct information on the charge density. In this case the initial core−hole state might be produced with different excitation sources spreading the possibilities for chemical speciation studies from synchrotron facilities also toward smaller laboratories. In addition, while XANES spectra collected in fluorescence mode are exposed to self-absorption effects leading to large uncertainties, the self-absorption does not influence the XES spectra of single-valence systems. However, in case of heterogeneous mixtures with large grain sizes above the absorption length, different self-absorptions of the mixed target constituents might influence also the accuracy of quantitative XES analysis. Finally, with the advent of the X-ray free electron laser (FEL) XES spectroscopy has been seriously considered as the most suitable technique for the electronic structure studies at FEL as it can be recorded on a single-shot basis and is not sensitive to the energy jitter of the self-amplified spontaneous emission (SASE) FEL pulse.[20,21]

The Kα and Kβ emission spectra of phosphorus induced with an X-ray tube or megaelectronvolt (MeV) proton beam[22−29] have been used by different authors to perform

Received: February 18, 2015
Accepted: April 30, 2015

DOI: 10.1021/acs.analchem.5b00782
Anal. Chem. XXXX, XXX, XXX−XXX

chemical speciation. Most of these works were interpreted using empirical methods, and only more recently it was demonstrated that XES spectroscopy can be applied for a true quantitative chemical speciation studies in combination with the ab initio quantum chemical calculations.[30,31] In current work we have extended our previous experimental and theoretical study of the sulfur K emission spectra[15,16] toward phosphorus and explore systematically the analytical capabilities of XES to extract information about the electronic structure of phosphorus in different compounds. High-resolution Kα and Kβ emission spectra of a series of phosphorus-containing compounds, including various oxidation states, structures, and ligand environments, were recorded. Two different independent sets of measurements were performed using synchrotron radiation and MeV proton beam for target excitation in order to verify that XES spectra are insensitive on the excitation mode. Quantum chemical calculations based on density functional theory[32] (DFT) were performed to obtain electron densities around phosphorus atom together with corresponding molecular orbitals and partial charges, which were then used to analyze the influence of chemical state and ligand environment on the measured spectra.

EXPERIMENTAL SECTION

Measurements of photoexcited and proton induced X-ray emission (PIXE) spectra were carried out at ID26 beamline of the European Synchrotron Radiation Facility (ESRF) and at the 2 MV tandem accelerator of the Jožef Stefan Institute in Ljubljana, respectively. In both experiments the Johansson-type crystal spectrometer for high-resolution spectroscopy in the tender X-ray range was used.[33] Target pellets pressed from powder reference materials purchased from Sigma-Aldrich were mounted on the motorized sample holder at 45° with respect to the incident beam while X-ray emission was collected perpendicular to the beam axis. In case of synchrotron measurements the incident photon beam was focused down to 250 × 50 μm^2, the photon energy was tuned to 3000 eV, and the flux on the target was ∼5 × 10^{12} photons/s. For PIXE measurements broad, unfocused proton beam with 8 × 8 mm^2 cross section was used. The proton energy was set to 2 MeV, and the total current was in the range 50−100 nA. In order to reach dispersive mode of operation, the target holder was placed inside the Rowland circle at the distance of 42.0 cm in front of the $(10\bar{1}0)$ SiO_2 analyzer crystal ($2d$ = 8.510 Å) and a position-sensitive charge-coupled device (CCD) detector was used. The position spectra recorded by the CCD detector were converted into energy scale using average Kα_1 line position of phosphate samples and the K$\beta_{1,3}$ line position of the K_3PO_4 target and corresponding reference energies of 2014.54[23] and 2138.0 eV,[27] respectively. The final experimental resolution at the energy of the phosphorus Kα line was 0.41 eV for the synchrotron radiation induced spectra, which was slightly decreased for PIXE spectra to 0.52 eV, mainly due to broad, unfocused beam used for target irradiation. During the acquisition of a series of Kα or Kβ spectra, the crystal and detector were kept at fixed position which enabled reliable measurements of small energy shifts. The energy bandwidth covered at this fixed position is given by the CCD width and was 44 and 56 eV for Kα and Kβ measurements, respectively. Possible systematic errors of measured energy shifts were examined by repeated measurements of several pellets of the same compound attached to different position on the sample holder. They were found to be within the precision limit of 0.027 eV. The count rate on the top of the Kα_1 line was around 60 counts/s for synchrotron measurements and approximately 30 times less for PIXE measurements, and the corresponding acquisition times of 500 and 2000 s were used. In case of Kβ emission lines the count rates were ∼30 times lower, so the total acquisition times were increased to 2500 s for the ESRF measurements and up to 3 h in case of PIXE experiment. While measured compounds with the highest formal oxidation state 5+ were completely stable, compounds with lower oxidation number were much more sensitive and changes of the oxidation state upon the irradiation could be observed. In order to avoid radiation damage and record reliable Kα spectra also for these samples, the incident photon flux was reduced by hundred times. In case of proton-induced spectra and also synchrotron radiation induced Kβ spectra, accumulations of short exposures from several fresh target spots were used to reach decent statistics also for samples with lower oxidation state.

THEORETICAL FRAMEWORK

Different approaches can be used to model the high-resolution XES spectra. The core−core transitions such as Kα spectra also reported in this work can be calculated with the charge-transfer multiplet approach.[34] This approach is not applicable for valence−core transitions where molecular orbital methods are usually applied. The discrete variational (DV) Xα molecular orbital theory was used by Adachi and Taniguchi[35] and later by Ceppi et al.[31] to model the Kβ emission spectra of some phosphate compounds in good agreement with the experiment. An alternative approach is the multiple scattering calculations implemented in the FEFF[36] code, and this was used by Ankudinov et al.[30] to model the Kβ emission spectra of P_2O_5 and P_2S_5 compounds. In this case the molecular orbitals are avoided and electronic structure information is obtained by projecting the calculated local density of states of the central atom. In our previous work on sulfur[15,16] the DFT was used to model successfully the measured spectra, calculate the electronic structure of S, and extract information about the chemical bonding in measured compounds. In addition, consistency between the DFT- and the FEFF-calculated mean number of valence electrons was confirmed. In current work we have kept the same framework and applied DFT method to further test the general applicability of this approach to XES analysis of low-Z elements.

Ab initio quantum chemical calculations of both Kα transition energies and Kβ emission spectra were performed with the StoBe-deMon molecular/cluster DFT code.[37] First, the geometry optimization of the first two coordination spheres around phosphorus atom was performed yielding the ground state of each molecule. In order to describe the character of corresponding molecular orbitals in terms of atomic orbitals, a Mulliken analysis[38−41] was performed. The obtained coordination of atoms around phosphorus was further on used to calculate the initial $1s^{-1}$ core hole state and final states with $2p^{-1}$ and the valence orbit hole corresponding to Kα and Kβ transition, respectively. In this procedure Kohn−Sham orbitals of the ground state were used to represent both initial and final states. The spontaneous dipole transitions were treated as an explicit one-electron transitions.[42,43] In order to increase the accuracy of the calculated transition energies, the energy difference between separately optimized initial and final states was computed. The orbital basis sets for H, O, and P atoms were (3111/111), (6311/311/1), and TZVP (73111/6111/1), respectively, and the exchange functional of Becke, Be88,[44] and

DOI: 10.1021/acs.analchem.5b00782
Anal. Chem. XXXX, XXX, XXX−XXX

the functional of Perdew, PD91,[45,46] were used for the correlation part.

RESULTS AND DISCUSSION

Phosphorus Kα Spectra. The Kα emission line corresponds to transition between deep atomic-like 2p and 1s orbitals and consequently the emitted spectra exhibit typical Lorentz-shaped atomic $K\alpha_{1,2}$ doublet structure. Since the emitted spectra correspond to core−core transition, the spectral shape does not depend on the chemical environment of the phosphorus atom and the valence orbital electron population influences the spectra only indirectly by screening the nuclear potential. When emission spectra are collected with high energy resolution on the level of natural lifetime broadening, tiny energy shifts of the measured lines are observed. Figure 1 exhibits $K\alpha_{1,2}$ emission spectra measured for

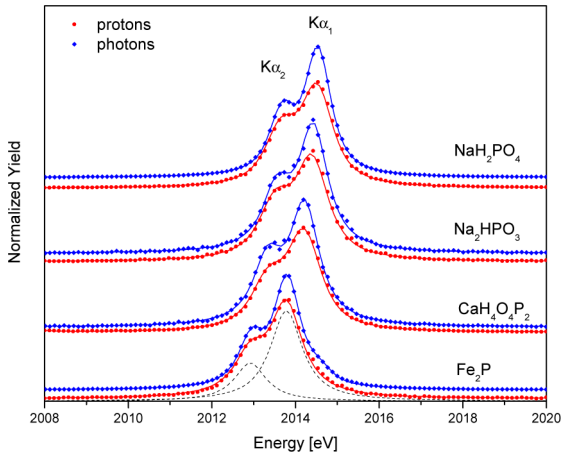

Figure 1. High-resolution P $K\alpha_{1,2}$ emission spectra of several phosphorus compounds with different formal oxidation number induced by synchrotron radiation and MeV proton beam.

phosphorus compounds with different formal oxidation number ranging from phosphide (P^{3-}) to phosphate (P^{5+}). Emission spectra induced by 3 keV monochromatic photon beam as well as 2 MeV proton beam are shown in Figure 1. Besides slightly higher energy resolution of the synchrotron radiation induced spectra both sets of spectra are practically the same.

Clear energy shifts are observed in measured spectra by increasing oxidation state going from phosphide to phosphate sample. In order to extract precise energies the measured spectra were fitted with two Voigt profiles, which are convolution of the Lorentzian natural line shape with the Gaussian profile corresponding to the response of the spectrometer. The same widths were used for both components in the fitting procedure. As also shown in Figure 1, such fitting model reproduces almost perfectly the measured spectra and $K\alpha_{1,2}$ energies can be extracted with high precision. Extracted emission energies for all measured compounds are tabulated in Table 1. The extracted spin orbit splitting of the two components is 0.87 ± 0.01 eV and is the same for all measured compounds, so only $K\alpha_1$ energies are given. Differences between extracted energies for photon and proton induced spectra are within the experimental uncertainties, so the average energy of both experiments is reported.

From tabulated energies a clear trend is observed depending on the oxidation state of phosphorus within the sample. The phosphorus Kα line position is shifted toward higher emission

Table 1. Experimental and Calculated Energy Positions of $K\alpha_1$ Lines of Various Phosphorus Compounds[a]

chemical formula	oxidation state	$K\alpha_1$[eV] measured	$K\alpha_1$[eV] calcd	DFT electron configuration
Fe_2P	3−	2013.80	2013.78	$3s^{1.66}3p^{2.97}3d^{0.11}$
$CaH_4O_4P_2$	1+	2014.22	2014.22	$3s^{1.10}3p^{2.50}3d^{0.41}$
Na_2HPO_3	3+	2014.43	2014.38	$3s^{0.89}3p^{2.40}3d^{0.52}$
$Al(PO_3)_3$	5+	2014.60		
$Ba(PO_3)_2$	5+	2014.52		
$CaFO_3P$	5+	2014.53	2014.44	$3s^{0.72}3p^{2.41}3d^{0.58}$
$K_3(PO_4)$	5+	2014.53	2014.46	$3s^{0.74}3p^{2.49}3d^{0.56}$
$KH_2(PO_4)$	5+	2014.52	2014.64	$3s^{0.72}3p^{2.31}3d^{0.58}$
$Na_2H(PO_4)$	5+	2014.55	2014.63	$3s^{0.73}3p^{2.39}3d^{0.57}$
$Na_4P_2O_7$	5+	2014.51		
$NaH_2(PO_4)$	5+	2014.54	2014.56	$3s^{0.75}3p^{2.32}3d^{0.57}$
$H_2O_2P^-$	1+		2014.32	$3s^{1.04}3p^{2.48}3d^{0.44}$
HPO_3^{2-}	3+		2014.43	$3s^{0.89}3p^{2.38}3d^{0.53}$
PO_4^{3-}	5+		2014.54	$3s^{0.70}3p^{1.79}3d^{0.54}$

[a]The DFT-based valence electron configuration is also given. The error of the measurements is 0.027 eV. The DFT-calculated values for each oxidation state including only the first coordination sphere around phosphorus atom are given at the bottom.

energy with increasing formal oxidation state. The energies for different samples with the same formal oxidation number 5+ practically match each other. An exception is the $Al(PO_3)_3$ exhibiting slightly higher energy, which may be explained with the large Al electronegativity compared to other metal ligands increasing slightly the phosphorus effective charge. Basically, the Kα line chemical energy shift is a clean and robust merit of the phosphorus oxidation state. On the absolute scale the measured energy shifts from phosphide (P^{3-}) to phosphate (P^{5+}) sample is only ∼0.8 eV which is relatively small value. However, due to a clean and simple doublet shape of the line which does not depend on the chemical state the Kα line energy can be determined with high precision. In addition the shape and energy position of emission spectra are not affected by target self-absorption and also do not depend on the excitation mode.

In order to enable more quantitative analysis DFT calculations of the Kα emission energies were performed. Since Kα line corresponds to core−core transition and the valence orbitals are not directly involved only the first coordination sphere around phosphorus atom including atoms directly bound to phosphorus was at first considered in our calculations. The calculated values for the Fe_2P single molecule and the $H_2O_2P^-$, HPO_3^{2-}, and PO_4^{3-} ions given at the bottom of Table 1 already reproduce very well the measured energy shifts. In order to provide also absolute energies which can be directly compared to experimental values given in Table 1 an overall shift of −1.16 eV was applied to all calculated energies. In the next step additional coordination spheres were included in calculations in order to account for the full molecule of each measured compound, and the final values are given in Table 1. Besides Kα emission energies also phosphorus valence electron configurations are given in Table 1. The latter were obtained by performing Mulliken population analysis on the DFT-calculated electron density. For some of the measured systems we were not able to achieve convergence in the calculations, so these values are missing. As shown in Figure 2, strong correlation can be observed between experimental $K\alpha_1$ emission energies and formal oxidation

DOI: 10.1021/acs.analchem.5b00782
Anal. Chem. XXXX, XXX, XXX−XXX

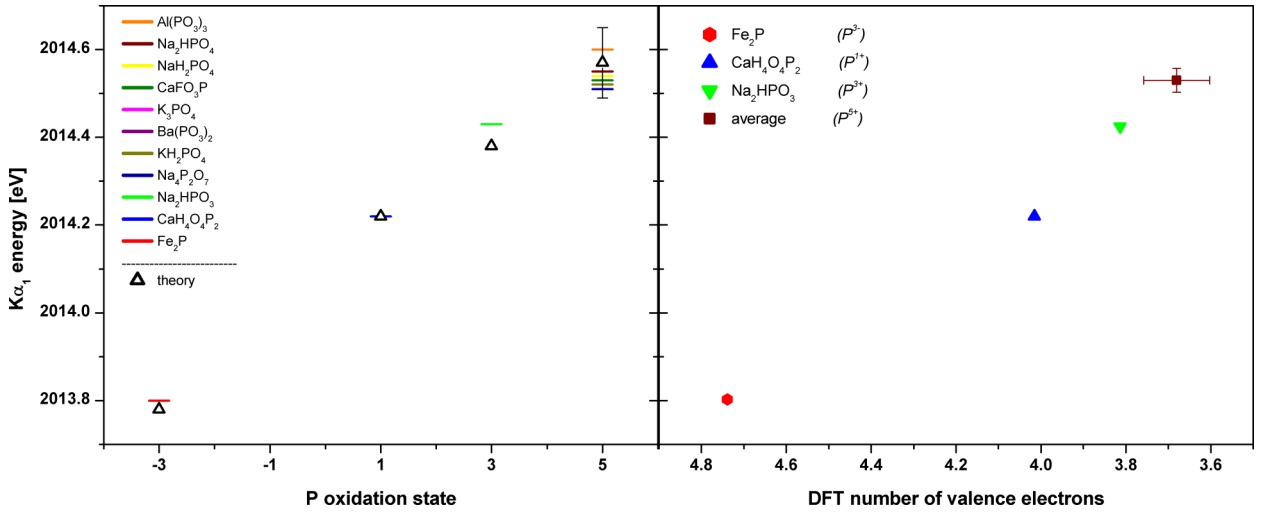

Figure 2. (Left) Experimental and theoretical P Kα_1 line energies vs formal oxidation state of P (right) and DFT-calculated number of valence electrons. For clarity only the average calculated value of phosphates is plotted with standard deviation of the calculated values given as error bars.

state of phosphorus and also with DFT-calculated number of valence electrons. With the use of synchrotron radiation for target excitation typical count rates in the order of 100 counts/s were obtained, so very good statistics is collected already within a few minutes. The detection limit can be estimated using typical peak to background ratio of 10^3 obtained with the $(10\bar{1}0)$ quartz analyzer crystal, which together with very high experimental energy resolution yielded final value of ~100−200 ppm within typical acquisition times of about 1 h. With dedicated high-efficiency XES spectrometer the detection limit can be pushed further down, and precise chemical state analysis employing energy analysis of the Kα emission spectra can be performed also on diluted P samples.

Phosphorus Kβ Spectra. While the Kα emission line corresponding to core−core transition reflects the valence electron density only indirectly by screening the nuclear potential, the Kβ emission spectrum arises as a result of the dipole transitions from the occupied molecular orbitals in the valence band to the atomic-like 1s orbital and therefore yield directly p-density of occupied valence state providing with high-sensitivity information on the chemical environment. The experimental Kβ emission spectra of three different phosphate compounds are shown in top part of Figure 4. Also in this case the measured spectra induced with photon and proton beam are basically the same; the main difference is only better statistics in the synchrotron radiation induced spectra due to higher incident photon flux. All measured phosphate spectra exhibit four main components traditionally labeled as K$\beta_{1,3}$, Kβ', Kβ_x, and Kβ''. While the characteristic structure composed of main K$\beta_{1,3}$ and Kβ' peaks remains the same, the intensity of the Kβ_x, and Kβ'' side peaks clearly increases with additional hydrogen atoms bound to the PO_4^{3-} ion.

In order to understand the spectral structure and also the influence of additional hydrogen atoms bound to the phosphate ion, DFT calculations of the electronic transitions corresponding to the phosphate Kβ emission spectrum were performed. The theoretical spectra were built from the calculated stick spectrum using Voigt profiles. The Gaussian width was fixed to 0.42 eV corresponding to experimental broadening while the Lorentzian width was increased with respect to the natural lifetime broadening to ~1.9 eV in order to describe experimentally observed line widths. An overall shift of the absolute energy scale of slightly less than −5 eV was applied to theoretical spectra in order to match the experimental energies. As a starting point only the first coordination sphere around phosphorus atom was considered, and the spectrum of the PO_4^{3-} ion was calculated and is presented in the bottom part of Figure 3. Mulliken analysis was also performed, and the corresponding atomic character of each separate molecular

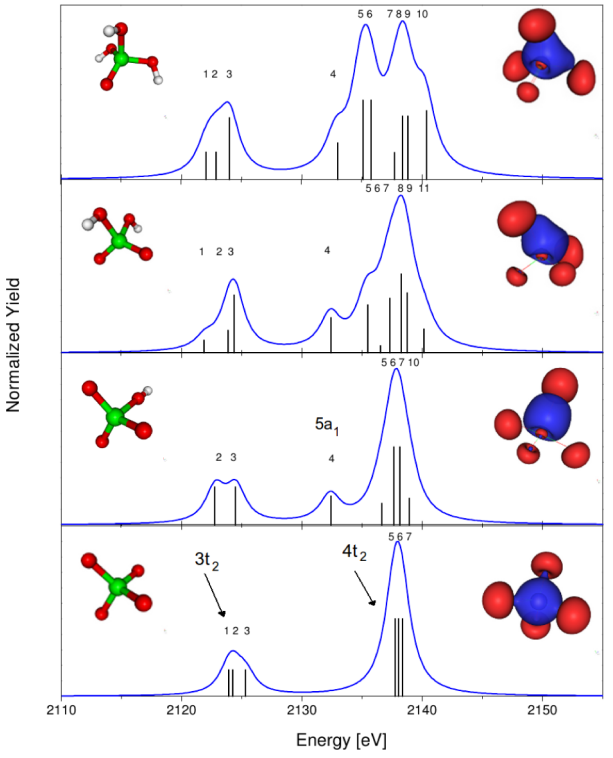

Figure 3. Theoretical spectra of (from bottom to top) PO_4^{3-}, HPO_4^{2-}, $H_2PO_4^{-}$, and H_3PO_4 phosphate ions. Geometrical structure of the molecule is presented on the left with green, red, and white representing the P, O, and H atoms, respectively. The development of the 4th ($5a_1$) orbital building the Kβ' peak is presented on the right side. The red and blue colors represent the negative and positive values of the wave function.

DOI: 10.1021/acs.analchem.5b00782
Anal. Chem. XXXX, XXX, XXX−XXX

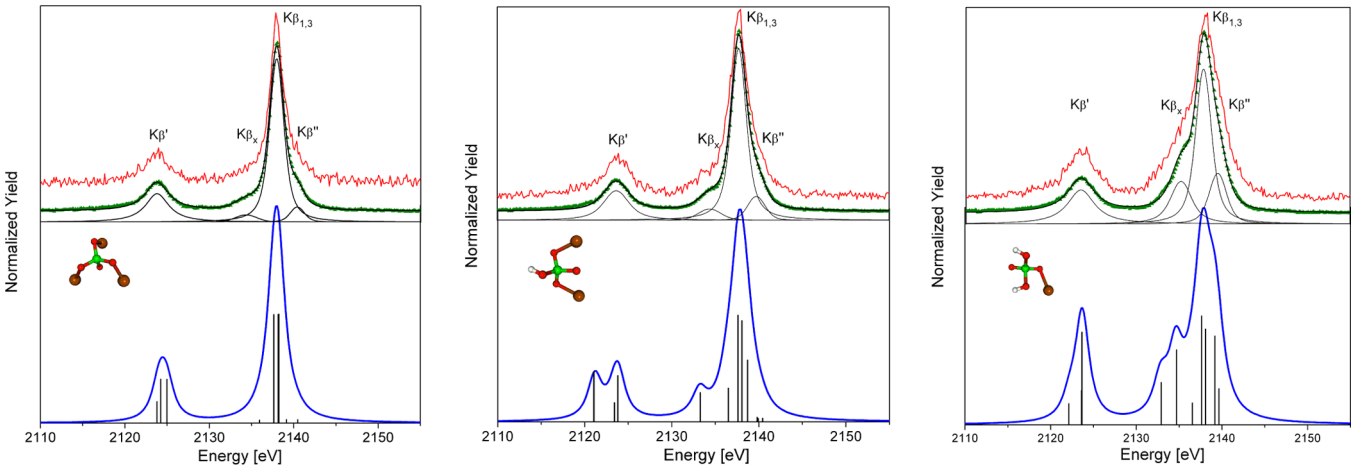

Figure 4. Experimental P Kβ emission spectra of (left) K_3PO_4, (center) Na_2HPO_4, and (right) NaH_2PO_4 induced with synchrotron radiation (green) and MeV protons (red) compared to theoretical model spectra (blue).

Table 2. Experimental Energies and Intensities of Main Spectral Components for the Phosphate Group along with the Average Atomic Character of the Group of Transitions Building the Model Spectra

	Kβ'	Kβ_x	K$\beta_{1,3}$	Kβ''
		K_3PO_4		
energy [eV]	2123.75(2)	2134.4(2)	2138.03(1)	2140.45(6)
intensity [au]	23.1(0.5)	3.8(1.0)	67.4(2.3)	5.7(1.2)
AO orbital	P3p 7	P3p 1	P3p 24	P3p 1
population [%]	P3d 2	P3s 27	O2s 10	P3d 3
	O2s 79	O2s 26	O2p 64	O2p 90
	O2p 3	O2p 44		K3s 4
	K3p 9			
		Na_2HPO_4		
energy [eV]	2123.61(2)	2134.5(2)	2137.80(1)	2139.82(8)
intensity [au]	19.9(0.5)	5.5(1.3)	65.7(3.4)	8.9(1.9)
AO orbital	P3p 6	P3p 6	P3p 19	P3p 5
population [%]	P3s 1	P3s 14	O2s 10	P3d 4
	P3d 1	O2s 15	O2p 66	O2p 86
	O2s 84	O2p 54	H1s 1	Na2p 3
	O2p 5	H1s 9		
		NaH_2PO_4		
energy [eV]	2123.40(2)	2135.27(1)	2137.90(4)	2139.5(1)
intensity [au]	20.7(0.5)	17.7(3.5)	46.0(7.9)	15.6(4.2)
AO orbital	P3p 5	P3p 8	P3p 15	P3p 5
population [%]	P3s 2	P3s 8	O2s 10	O2s 4
	O2s 84	O2s 9	O2p 70	O2p 89
	O2p 5	O2p 62	H1s 2	
	H1s 1	H1s 11		
		KH_2PO_4		
energy [eV]	2123.50(2)	2135.4(1)	2138.00(4)	2139.4(5)
intensity [au]	21.1(0.5)	14.9(4.0)	48.1(11.4)	15.9(7.9)
AO orbital	P3p 5	P3p 8	P3p 15	P3p 4
population [%]	P3s 1	P3s 8	O2s 9	P3d 2
	O2s 83	O2s 9	O2p 69	O2p 90
	O2p 5	O2p 61	H1s 2	H1s 1
	H1s 1	H1s 11		

orbital contributing to the model spectrum is given in Supporting Information.

The structure of the valence band reflects the tetrahedral molecular geometry of the PO_4^{3-} ion. Valence molecular orbitals are built of O2s, 2p and P3s, 3p, 3d atomic orbitals and are labeled according to the irreducible representations of the T_d point group: $4a_1^2$, $3t_2^6$, $5a_1^2$, $4t_2^6$, $1e^4$, $5t_2^6$, and $1t_1^6$. Among these only t_2 orbitals contribute to the Kβ emission spectrum since by the dipole selection rule transitions into 1s level are allowed only from the orbitals of t_2 symmetry. As seen from Figure 3 already the theoretical PO_4^{3-} spectrum yields two main spectral components in good agreement with the experiment. The Kβ' component corresponds to transition from the $3t_2$ and K$\beta_{1,3}$ from the $4t_2$ molecular orbital. The $3t_2$ MO is mainly composed

DOI: 10.1021/acs.analchem.5b00782
Anal. Chem. XXXX, XXX, XXX−XXX

of P3p and O2s and $4t_2$ MO of P3p and O2p atomic orbitals. The calculated intensity for transitions from $5t_2$ MO which could produce the Kβ'' spectral component were in case of pure PO_4^{3-} ion more than 100 times weaker in comparison with transitions from $4t_2$ building the main K$\beta_{1,3}$ component, and they do not contribute significantly to the theoretical spectrum.

In order to explain also both side peaks Kβ_x and Kβ'' and its dependence on the number of hydrogen atoms bound to PO_4^{3-} ion observed in experimental spectra we have expanded the calculations to include also the next coordination shell. With additional hydrogen atoms bound to PO_4^{3-} ion the original tetrahedral T_d symmetry is broken leading to different mixing of the atomic orbitals and changing the dipole transition matrix elements that contribute to the spectrum. In principle, one cannot label the orbitals according to the irreducible representations of the T_d point group any more, but in order to keep the same number of electrons and follow each orbital only additional protons were actually introduced in our theoretical model and, consequently, same labels were used. By adding additional protons the theoretical spectrum starts to develop both side peaks which also grow in intensity with increasing number of hydrogens in agreement with experimental observation.

The Kβ_x contribution on the low-energy tail of the main K$\beta_{1,3}$ peak is explained as transition from the $5a_1$ orbital which changes its atomic character yielding significant amount of P3p contribution. In a similar way also Kβ'' contribution on the high-energy side of the main K$\beta_{1,3}$ peak is explained as transition from 1e orbital which also changes its atomic character with large amount of P3p contribution. In addition also the intensity of transitions from $5t_2$ orbitals is increased compared to the PO_4^{3-} ion. So our calculations qualitatively reproduce the measured phosphate spectra and also explain the increasing intensity of Kβ_x and Kβ'' side peaks depending on the number of hydrogens bound to the PO_4^{3-} ion. We have not recorded also the H_3PO_4 spectrum, but our calculations reproduce well the spectrum measured by Sugiura.[25]

Finally, the theoretical model spectra for three typical measured phosphates taking into account a full molecule are presented in Figure 4 and compared to the experimental spectra. The latter were fitted with four Voigt profiles in order to extract energies and relative intensities of the main spectral components, and the fitted spectrum is also shown in Figure 4. The extracted values are tabulated in Table 2 together with the atomic character of each spectral contribution. This character was obtained by performing Mulliken analysis and averaging the atomic characters of separate molecular orbitals contributing to the particular spectral component. We can see that the influence of the cation on the K_3PO_4 spectrum profile is almost negligible and the spectrum is very similar to the PO_4^{3-} model. On the other hand large effects of hydrogen atoms bound to the phosphate ion are observed, as already discussed above. Because of ionic bonding with potassium, a valence electron is transferred to the phosphate ion resulting in an almost pure PO_4^{3-} spectrum. In case of the covalent bonding with hydrogen, the electron is shared with the phosphate perturbing significantly the valence molecular orbitals contributing to the Kβ emission spectrum.

Similar analysis can be performed for the compounds with lower-symmetry field (C_{3v} and C_{2v}) with direct bonding of hydrogen atoms to phosphorus. Experimental Kβ emission spectra of Na_2HPO_3 and $CaH_4O_4P_2$ and the comparison with theoretical model are presented in Figure 5. Both spectra

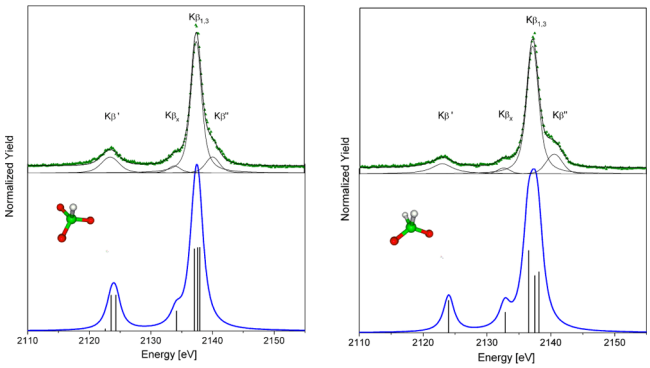

Figure 5. Experimental (green) P Kβ emission spectra of (top) Na_2HPO_3 and (bottom) $CaH_4O_4P_2$ compared to theoretical model spectra (blue) calculated for the HPO_3^{2-} and the $H_2PO_2^-$ ions, respectively.

exhibit similar structure as the phosphate spectra and are composed of four main spectral components. Also in this case we have fitted the spectra by Voigt profiles. The energies and relative intensities of the main spectral components were extracted and are tabulated in Table 3 together with the atomic character of each spectral contributions based on the Mulliken analysis. The calculations fail to reproduce the spectral component Kβ'' on the high-energy shoulder of the main K$\beta_{1,3}$ peak, so the atomic character for this particular contribution is not given in Table 3. Besides the Kβ'' component our calculations reproduce well the measured spectra. An observed decrease of the Kβ'/K$\beta_{1,3}$ intensity ratio by going from $HPO_3^{2-} \rightarrow H_2O_2P^-$ is well-explained by the calculations. While the predominant P3p and O2s character of the group of molecular orbitals corresponding to the Kβ' component is very similar in both compounds, the number of oxygen atoms is simply reflected in the relative intensity of the Kβ' component. Our calculations throughout this work have been restricted to model a single isolated molecule. As we have seen, such model is already able to reproduce quite well experimental spectra and explain the main spectral features. However, in some cases larger cluster of atoms would be necessary which would change the configuration of molecular orbitals building the emission spectrum.

CONCLUSIONS

High energy resolution Kα and Kβ X-ray emission spectra can be used as a sensitive probe of a local electronic structure of phosphorus. Spectral features, e.g., energy position and spectral shape, are independent of the type of excitation. The Kα emission spectra exhibit characteristic atomic-like K$\alpha_{1,2}$ doublet structure; small energy shifts are observed which are correlated with the formal and also theoretical valence electron number (density) and can be used as a precise and robust merit of the phosphorus oxidation state. Chemical sensitivity is increased in Kβ emission spectra yielding the information about bonding, ligand type, and symmetry. Measured spectra were reproduced with the DFT calculations, and the influence of hydrogen atoms was identified within the phosphate series. Together with our previous work on S this study confirms that such approach is generally applicable to low-Z elements and XES spectroscopy can be used complementary to XANES technique to extract the information on their electronic structure. Finally, XES spectroscopy is probing the occupied states and it can be performed also with laboratory excitation sources. Recently, also X-ray

DOI: 10.1021/acs.analchem.5b00782
Anal. Chem. XXXX, XXX, XXX−XXX

Table 3. Experimental Energies and Intensities of the Main Spectral Components for Na_2HPO_3 and $CaH_4O_4P_2$ Together with the Average Atomic Character of the Group of Transitions Building Up the Model Spectra

	Kβ'	Kβ_x	K$\beta_{1,3}$	Kβ''
		HPO_3^{2-}		
energy [eV]	2123.33(5)	2133.9(1)	2137.46(1)	2140.11(9)
intensity [au]	13.6(0.8)	4.2(1.4)	72.2(3.0)	10.0(1.8)
AO orbital	P3p 9	P3p 7	P3p 24	
population [%]	P3d 2	P3s 30	O2s 8	
	O2s 85	O2s 20	O2p 61	
	O2p 4	O2p 22	H1s 5	
		H1s 19		
		$H_2PO_2^-$		
energy [eV]	2122.87(7)	2132.7(1)	2137.22(1)	2140.59(5)
intensity [au]	12.3(0.8)	3.0(0.9)	72.2(1.5)	12.4(1.0)
AO orbital	P3p 12	P3p 10	P3p 29	
population [%]	O2s 81	P3s 40	O2s 8	
	O2p 4	O2s 15	O2p 46	
		O2p 6	H1s 15	
		H1s 27		

tube-based instrumentation for XAS spectroscopy in the transmission mode has been introduced, and the complementary character of both techniques can be now exploited in the laboratory analysis.

■ ASSOCIATED CONTENT

Supporting Information

The results of the Mulliken analysis yielding atomic character of separate molecular orbitals building the model Kβ emission spectra. The Supporting Information is available free of charge on the ACS Publications website at DOI: 10.1021/acs.analchem.5b00782.

■ AUTHOR INFORMATION

Corresponding Authors

*E-mail: matjaz.kavcic@ijs.si.
*E-mail: m.petric@ijs.si.

Notes

The authors declare no competing financial interest.

■ ACKNOWLEDGMENTS

This work has been supported by Marie Curie Actions−Initial Training Networks (ITN) as an Integrating Activity Supporting Postgraduate Research with Internships in Industry and Training Excellence (SPRITE) under EC contract no. 317169. A part of the work has been supported also by the SPIRIT EC project under contract no. 227012. Finally, the authors acknowledge the support of the Slovenian Research Program P1-0112 and an excellent assistance of the ID26 beamline staff in preparation of the synchrotron experiment.

■ REFERENCES

(1) Westheimer, F. *Science* **1987**, *235*, 1173−1178.
(2) Benitez-Nelson, C. R. *Earth-Sci. Rev.* **2000**, *51*, 109−135.
(3) Heckrath, G.; Brookes, P. C.; Poulton, P. R.; Goulding, K. W. T. *J. Environ. Qual.* **1995**, *24*, 904.
(4) Eghball, B.; Binford, G. D.; Baltensperger, D. D. *J. Environ. Qual.* **1996**, *25*, 1339.
(5) Anderson, L.; Faul, K.; Paytan, A. *Mar. Chem.* **2010**, *120*, 44−56.
(6) Paytan, A.; McLaughlin, K. *Chem. Rev.* **2007**, *107*, 563−576.
(7) Peak, D.; Sims, J. T.; Sparks, D. L. *Environ. Sci. Technol.* **2002**, *36*, 4253−4261.
(8) Beauchemin, S.; Hesterberg, D.; Chou, J.; Beauchemin, M.; Simard, R. R.; Sayers, D. E. *J. Environ. Qual.* **2003**, *32*, 1809.
(9) Sato, S.; Solomon, D.; Hyland, C.; Ketterings, Q. M.; Lehmann, J. *Environ. Sci. Technol.* **2005**, *39*, 7485−7491.
(10) Shober, A. L.; Hesterberg, D. L.; Sims, J. T.; Gardner, S. *J. Environ. Qual.* **2006**, *35*, 1983.
(11) Diaz, J.; Ingall, E.; Benitez-Nelson, C.; Paterson, D.; de Jonge, M. D.; McNulty, I.; Brandes, J. A. *Science* **2008**, *320*, 652−655.
(12) Brandes, J. A.; Ingall, E.; Paterson, D. *Mar. Chem.* **2007**, *103*, 250−265.
(13) Seiter, J. M.; Staats-Borda, K. E.; Ginder-Vogel, M.; Sparks, D. L. *J. Environ. Qual.* **2008**, *37*, 477.
(14) Ingall, E. D.; Brandes, J. A.; Diaz, J. M.; de Jonge, M. D.; Paterson, D.; McNulty, I.; Elliott, W. C.; Northrup, P. *J. Synchrotron Radiat.* **2011**, *18*, 189−197.
(15) Alonso Mori, R.; Paris, E.; Giuli, G.; Eeckhout, S. G.; Kavčič, M.; Žitnik, M.; Bučar, K.; Pettersson, L. G. M.; Glatzel, P. *Anal. Chem.* **2009**, *81*, 6516−6525.
(16) Mori, R. A.; Paris, E.; Giuli, G.; Eeckhout, S. G.; Kavčič, M.; Žitnik, M.; Bučar, K.; Pettersson, L. G. M.; Glatzel, P. *Inorg. Chem.* **2010**, *49*, 6468−6473.
(17) Smolentsev, G.; et al. *J. Am. Chem. Soc.* **2009**, *131*, 13161−13167.
(18) Lancaster, K. M.; Roemelt, M.; Ettenhuber, P.; Hu, Y.; Ribbe, M. W.; Neese, F.; Bergmann, U.; DeBeer, S. *Science* **2011**, *334*, 974−977.
(19) Szlachetko, J.; et al. *Chem. Commun.* **2012**, *48*, 10898−10900.
(20) Alonso-Mori, R.; et al. *Proc. Natl. Acad. Sci. U. S. A.* **2012**, *109*, 19103−19107.
(21) Kern, J.; et al. *Science* **2013**, *340*, 491−495.
(22) Takahashi, Y. *Bull. Chem. Soc. Jpn.* **1972**, *45*, 4−7.
(23) Fichter, M. *Spectrochim. Acta, Part B* **1975**, *30*, 417−431.
(24) Taniguchi, K. *Bull. Chem. Soc. Jpn.* **1984**, *57*, 909−914.
(25) Sugiura, C. *J. Phys. Soc. Jpn.* **1995**, *64*, 848−857.
(26) Sugiura, C. *J. Phys. Soc. Jpn.* **1995**, *64*, 2510−2523.
(27) Sugiura, C.; Yorikawa, H.; Muramatsu, S. *J. Phys. Soc. Jpn.* **1996**, *65*, 2940−2945.
(28) Deluigi, M. T.; Perino, E.; Olsina, R.; de la Vega, A. R. *Spectrochim. Acta, Part B* **2003**, *58*, 1699−1707.
(29) Tada, T.; Fukuda, H.; Hasegawa, J.; Oguri, Y. *Spectrochim. Acta, Part B* **2010**, *65*, 46−50.
(30) Ankudinov, A. L.; Elam, W. T.; Sieber, J. R.; Rehr, J. J. *X-Ray Spectrom.* **2006**, *35*, 312−318.
(31) Ceppi, S.; Tirao, G.; Stutz, G.; Riveros, J. A. *Chem. Phys.* **2008**, *354*, 80−85.
(32) Kohn, W. *Rev. Mod. Phys.* **1999**, *71*, 1253−1266.

DOI: 10.1021/acs.analchem.5b00782
Anal. Chem. XXXX, XXX, XXX−XXX

(33) Kavčič, M.; Budnar, M.; Mühleisen, A.; Gasser, F.; Žitnik, M.; Bučar, K.; Bohinc, R. *Rev. Sci. Instrum.* **2012**, *83*, 069901.
(34) de Groot, F.; Kotani, A. *Core Level Spectroscopy of Solids*; Taylor and Francis: New York, 2008; Vol. *6*.
(35) Adachi, H.; Taniguchi, K. *J. Phys. Soc. Jpn.* **1980**, *49*, 1944−1953.
(36) Ankudinov, A. L.; Ravel, B.; Rehr, J. J.; Conradson, S. D. *Phys. Rev. B* **1998**, *58*, 7565−7576.
(37) Hermann, K.; et al. *StoBe-deMon*, version 3.1., 2011; http://www.fhi-berlin.mpg.de/KHsoftware/StoBe/index.html.
(38) Mulliken, R. S. *J. Chem. Phys.* **1955**, *23*, 2338−2342.
(39) Mulliken, R. S. *J. Chem. Phys.* **1955**, *23*, 2343−2346.
(40) Mulliken, R. S. *J. Chem. Phys.* **1955**, *23*, 1833−1840.
(41) Mulliken, R. S. *J. Chem. Phys.* **1955**, *23*, 1841−1846.
(42) Nilsson, A.; Pettersson, L. G. M. *Surf. Sci. Rep.* **2004**, *55*, 49−167.
(43) Föhlisch, A.; Hasselström, J.; Bennich, P.; Wassdahl, N.; Karis, O.; Nilsson, A.; Triguero, L.; Nyberg, M.; Pettersson, L. G. M. *Phys. Rev. B* **2000**, *61*, 16229−16240.
(44) Becke, A. *Phys. Rev. A* **1988**, *38*, 3098−3100.
(45) Perdew, J.; Wang, Y. *Phys. Rev. B* **1992**, *45*, 13244−13249.
(46) Perdew, J.; Chevary, J.; Vosko, S.; Jackson, K.; Pederson, M.; Singh, D.; Fiolhais, C. *Phys. Rev. B* **1992**, *46*, 6671−6687.

DOI: 10.1021/acs.analchem.5b00782
Anal. Chem. XXXX, XXX, XXX−XXX